Processes Governing the Ablation of Intercepted Snow

Alex C. Cebulski[1], **John W. Pomeroy**[1]

[1]Centre for Hydrology, University of Saskatchewan, Canmore, Canada,

Key Points:

- Unloading was found to be strongly associated with canopy snow load, wind shear stress, and canopy snowmelt.
- Implementation of a new model that includes both melt and dry snow unloading processes improved canopy snow load predictions.
- The fraction of snowfall sublimated in the canopy differed by up to a factor of three across existing models.

Corresponding author: Alex C. Cebulski, alex.cebulski@usask.ca

Abstract

Interception and ablation of snow in forest canopies significantly influence the quantity, timing, and phase of precipitation that reaches the ground in cold regions forests. Yet current modelling approaches have uncertain transferability across differing climate and forest types, often omit key processes, and typically couple interception and ablation processes in ways that limit both process representation and evaluation. Here, in-situ observations from a needleleaf forest in the Canadian Rockies are utilised to evaluate the theories underpinning existing canopy snow ablation models and develop novel understanding to support the development of a new canopy snow ablation model. The observations revealed that canopy snow load, wind shear stress, and canopy snowmelt were strongly associated with unloading; however, air temperature and sublimation were not. A new canopy snow ablation model was developed based on these associations and their impact on the canopy snow energy and mass balance. This model demonstrated improved performance in simulating canopy snow load relative to previous approaches, especially for melt- and wind-dominated ablation events. The improved performance in representing canopy snow load compared to existing models results from including energy balance-based melt and dry snow unloading relationships with snow load and wind shear stress. The inclusion of both melt and dry snow unloading processes in the new model also led to more consistent partitioning of snowfall to the atmosphere versus the ground compared to existing approaches across a wide range of meteorologies.

1 Introduction

The seasonal snowpack is an essential component of global water resources (Immerzeel et al., 2020; Viviroli et al., 2020) and is increasingly threatened by rapid climate and land cover change (Aubry-Wake & Pomeroy, 2023; Fang & Pomeroy, 2023; López-Moreno et al., 2014; Szczypta et al., 2015). Vegetation cover can significantly alter the quantity (Essery et al., 2003; Pomeroy & Gray, 1995; Sanmiguel-Vallelado et al., 2020) and timing (Ellis et al., 2010; Safa et al., 2021) of snow that reaches the ground. Forest canopies cover more than half of the snow-covered area in the Northern Hemisphere (Kim et al., 2017), making forest-snow interactions crucial to understand for informed ecological, land management, and water resource decision-making. Needleleaf canopies are particularly effective at intercepting snowfall (Cebulski & Pomeroy, 2025b; Hedstrom & Pomeroy, 1998; Pomeroy & Schmidt, 1993; Storck et al., 2002), where intercepted snow is subject to increased energy inputs relative to the subcanopy snowpacks, leading to increased rates of melt, unloading, and/or sublimation (Parviainen & Pomeroy, 2000; Pomeroy et al., 1998b; Roesch et al., 2001; Storck et al., 2002). The partitioning of snow to the atmosphere via sublimation (Parviainen & Pomeroy, 2000; Pomeroy et al., 1998b) or to the ground through unloading and meltwater drip (Lumbrazo et al., 2022; Roesch et al., 2001; Storck et al., 2002) is highly sensitive to meteorological conditions and forest structure contributing to substantial variability in subcanopy snowpacks across regions and snowfall events. Coastal humid environments typically exhibit small sublima-

tion losses and a larger influence of unloading and melt (Floyd, 2012; Storck et al., 2002). Here, enhanced canopy energy inputs combined with high humidity increases both solid snow unloading and melt of snow intercepted in the canopy (Lumbrazo et al., 2022; Lundquist et al., 2021; Roesch et al., 2001). Conversely, the colder and drier winters in continental climates typical of the boreal forests can induce substantial canopy sublimation losses (e.g., 25—45% of annual snowfall in Essery et al., 2003) in addition to unloading (Essery et al., 2003; Gelfan et al., 2004; Parviainen & Pomeroy, 2000; Pomeroy et al., 1998b, 2002). As a result, reliable models of snow accumulation and streamflow in forested basins rely on a comprehensive understanding of interception processes (Clark et al., 2015; Essery et al., 2003; Pomeroy et al., 1998a; Verseghy, 2017; Wheater et al., 2022).

Canopy snow models have demonstrated variable transferability across different climates and forest types (Essery et al., 2003; Gelfan et al., 2004; Lumbrazo et al., 2022; Lundquist et al., 2021), and uncertainty in transferability has been attributed as a key area limiting the performance in predicting forest snowpacks in hydrological model intercomparisons (Krinner et al., 2018; Rutter et al., 2009). Recent studies have emphasized the importance of distinguishing between initial snow interception and subsequent ablation processes (Cebulski & Pomeroy, 2025a; Cebulski & Pomeroy, 2025b). This separation allows for individual parameterisations for distinct processes, improving both process representation and the modular design of contemporary models, thereby supporting broader applicability across diverse environments and model structures (Clark et al., 2015; Pomeroy et al., 2022). In addition, Lundquist et al. (2021) and Cebulski & Pomeroy (2025b) demonstrated that canopy snow processes can be more accurately represented without the concept of a maximum canopy snow load, which is included in initial accumulation parameterisations (Andreadis et al., 2009; Hedstrom & Pomeroy, 1998). Existing ablation routines were integrated in canopy snow accumulation parameterisations, likely as a result of some ablation included in measurements of interception efficiency (Cebulski & Pomeroy, 2025a). For example, Hedstrom & Pomeroy (1998) found that interception efficiency declined as the canopy is loaded with snow, while Storck et al. (2002) found a constant interception efficiency of 0.6 and is also typically combined with a maximum canopy snow load. Consequently, both the Hedstrom & Pomeroy (1998) and Storck et al. (2002) parameterisations have significantly lower interception efficiencies—prior to canopy snow ablation—compared to the observations by Cebulski & Pomeroy (2025b). Staines & Pomeroy (2023) and Cebulski & Pomeroy (2025b) show that interception efficiency is best predicted by canopy density alone—consistent with some rainfall interception parameterisations (e.g., Valante et al.,

1997; Zhong et al., 2022)—and that snow load has a small influence on canopy density, challenging the Hedstrom & Pomeroy (1998) and Storck et al. (2002) initial snow interception theories. Together these studies (Cebulski & Pomeroy, 2025a; Cebulski & Pomeroy, 2025b; Lundquist et al., 2021) emphasize the need to revisit canopy snow ablation parameterisations.

Ablation of intercepted snow due to snow unloading to the ground has previously been shown to be associated air temperature (Katsushima et al., 2023; Roesch et al., 2001; Schmidt & Pomeroy, 1990), ice-bulb temperature—which more accurately represents the cooling effect of sublimation compared to air temperature—(Ellis et al., 2010; Floyd, 2012), canopy snowmelt rate (Storck et al., 2002), and wind speed as shown in Figure 1 for (Bartlett & Verseghy, 2015; Katsushima et al., 2023; Roesch et al.; 2001, 2001). Each of these factors were also found to be dependent on canopy snow load and time (Figure 1). While Hedstrom & Pomeroy (1998) did not make direct observations of canopy snow unloading, they proposed a parameterisation based on canopy snow load and time. In addition to the empirical observations by the afformentioned studies, physical reasoning also supports the inclusion of these processes. For example, melt promotes unloading through loss of structural integrity, particle bond weakening, and lubrication of intercepted snow. Wind drag promotes unloading through shear stress applied to intercepted snow, wind erosion through direct entrainment in the atmosphere of intercepted snow, and branch movement. Branch elasticity increases with temperature (Schmidt & Pomeroy, 1990) which can increase the likelihood of unloading due to increasing branch angle under a snow load and decreased stiffness to resist swaying in a turbulent wind.

Melt of snow intercepted in the canopy is typically represented by either an energy balance approach (Andreadis et al., 2009; Clark et al., 2015; e.g., Parviainen & Pomeroy, 2000), as a function of air temperature (Roesch et al., 2001), or a function of ice-bulb temperature (Ellis et al., 2010; Floyd, 2012) (Figure 2). Sublimation is generally represented using a coupled energy and mass balance approach (e.g., Essery et al., 2003; Pomeroy et al., 1998b; Verseghy, 2017). The Essery et al. (2003) and Pomeroy et al. (1998b) approaches differ in that Pomeroy et al. (1998b) does not include longwave radiation in the canopy snow energy balance. Both the Essery et al. (2003) and Pomeroy et al. (1998b) parameterisations decrease the latent heat flux from snow intercepted in the canopy as the canopy fills up with snow and its specific surface area decreases. However, these parameterisations are based on estimates of maximum canopy snow load which may underestimate true maxima (Cebulski & Pomeroy, 2025b; Lundquist et al., 2021; Storck et al., 2002) and should

be reconsidered using a larger maximum load or an approach that avoids prescribing a maximum load. The merits of including more physically based energy balance methods compared to more empirically based functions for calculating snowmelt and sublimation have not been directly assessed using an event-based process investigation.

Quantifying individual canopy snow ablation processes including unloading, wind redistribution, melt, drip, and sublimation remains challenging, even with sophisticated lysimetry (Storck et al., 2002) and eddy-covariance systems (Conway et al., 2018; Harding & Pomeroy, 1996; Harvey et al., 2025). Consequently, some canopy snow ablation parameterisations have been developed using methods, such as above canopy albedo, which do not distinguish individual processes (Bartlett & Verseghy, 2015; Roesch et al., 2001). While these approaches offer useful indices of model performance, they provide limited insight into the accuracy of individual process representations. Lysimeter-based measurements offer more direct process-level observations, but interpretation of their observations is made uncertain by freeze–thaw cycles and concurrent processes (Floyd, 2012; MacDonald, 2010; Storck et al., 2002). A hybrid diagnostic approach that combines individual process measurements with simulations and employs observations such as canopy snow load from a weighed tree has yet to be applied but is explored in this study.

The objective of this study is to better understand and predict the influences of meteorology and snow load on intercepted snow ablation. This study specifically looks at canopy snow ablation after snowfall and initial interception. Cebulski & Pomeroy (2025b) has addressed processes governing the initial accumulation of snow in the canopy.

The specific research questions this research aims to address include:

1. How do air temperature, humidity, wind exposure, canopy snow sublimation, and snowmelt influence the rate of canopy snow unloading?

2. To what extent do current theoretical models of canopy snow ablation align with detailed in-situ observations?

3. What modifications to existing models, are necessary to accurately represent ablation of snow intercepted in the canopy and what is the improvement in performance from these modifications?

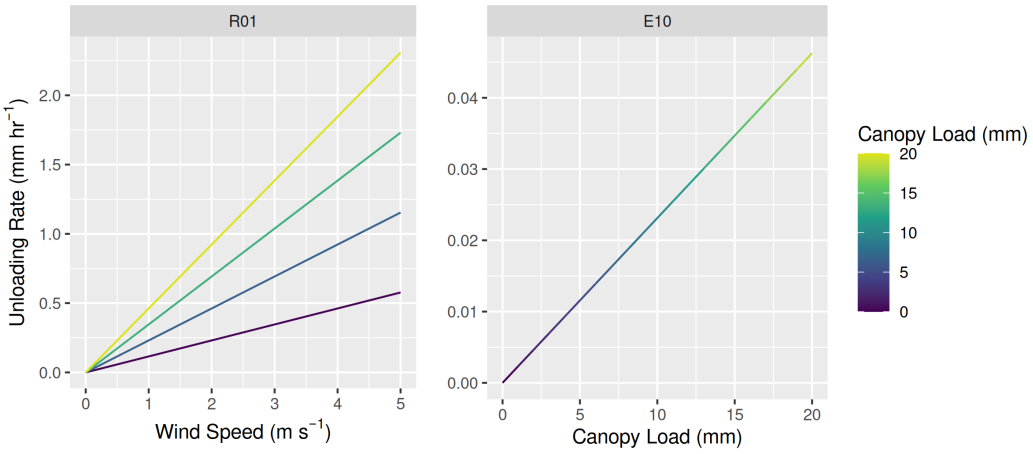

Figure 1: The Roesch et al. (2001) model of unloading rate with increasing wind speed and canopy snow load (left, R01) and the Hedstrom & Pomeroy (1998) model of unloading rate with increasing snow load (right, E10). Both examples have a constant air temperature of -10°C to disable the influence of warming on unloading and drip.

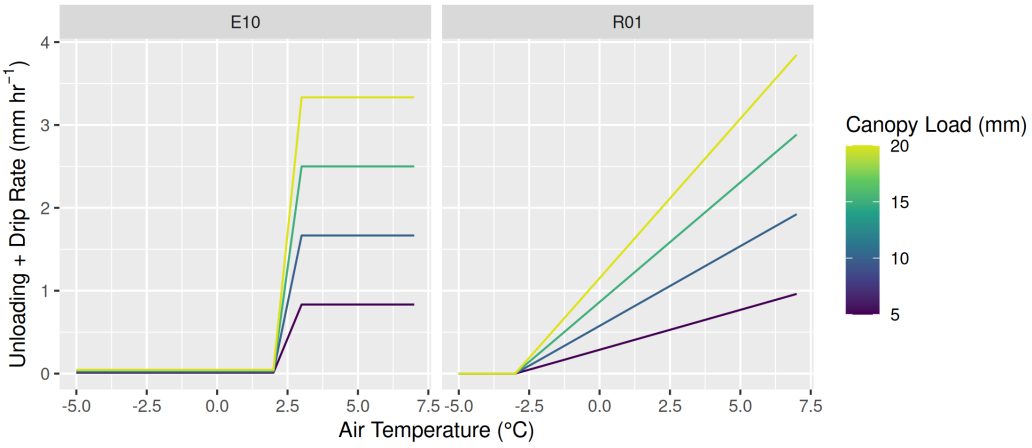

Figure 2: The Ellis et al. (2010) and Floyd (2012) (E10) model of unloading and drip rate (left) and the Roesch et al. (2001) (R01) model of unloading rate (right) with increasing air temperature. Wind speed for the R01 parameterisation was set to zero.

2 Methods

2.1 Study Site

The observations presented in this study were collected at Fortress Mountain Research Basin (FMRB), Alberta, Canada, -115° W, 51° N, a continental headwater basin in the Canadian Rockies. The site is located 2100 m above sea level on a ridge covered by mature fir and spruce forest. Air temperature, humidity, and wind speed were measured at a height of 4.3 m at Forest Tower (FT) Station (Figure 3). Shear stress was calculated using the EddyPro software (LI-COR Biosciences) based on high-frequency wind measurements from a CSAT3 three-dimensional sonic anemometer (Campbell Scientific) installed at 3.0 m at FT station. The CSAT3 was occasionally covered in snow during the analysis period, and thus to provide a complete record of shear stress, a linear relationship was established between shear stress derived from the CSAT3 and the square of wind speed measured at 4.3 m at the FT station ($R^2 = 0.71$, $p < 0.05$). This relationship was then used to gap-fill shear stress during periods when the CSAT3 was snow-covered. The precipitation rate was measured by an Alter-shielded OTT Pluvio weighing precipitation gauge installed 2.6 m above ground at the adjacent Powerline (PWL) Station (Figure 3). Incoming and outgoing solar radiation was measured by a Kipp & Zonen CNR4 4-Component Net Radiometer installed 3.27 m above the ground at Fortress Ridge Station (FRS) 2.0 km to the northwest of FT station (-115.2° W, 50.8° N). This windy exposed site was selected to reduce snow accumulation on the radiometers, in addition to the CNR4's built-in heating element. Three subcanopy lysimeters, consisting of plastic horse-watering troughs with an opening of 0.9 m^2 and depth of 20 cm suspended from a load cell, were installed to measure subcanopy snow accumulation. A weighed tree lysimeter (subalpine fir) suspended from a load cell (Artech S-Type 20210-100) measured the weight of canopy snow load (kg) and was scaled to an areal estimate of snow load (mm) using snow surveys as in Pomeroy & Schmidt (1993). To isolate the subcanopy lysimeter measurements of canopy snow unloading from throughfall, 15-min intervals were selected that had no atmospheric precipitation based on the precipitation gauge at PWL. The weighed tree and timelapse imagery also were used to confirm there was no atmospheric precipitation and to identify periods where snow was intercepted in the canopy and ablation was possible. Four tipping bucket rain gauges—3 Texas Electronics TR-525M and 1 Hyquest Solutions TB4MM—were installed along a 15 m transect adjacent to the dense canopy subcanopy lysimeter to quantify sub-canopy drip from melting intercepted snow. Additional details on this study site and the meteorological and lysimeter measurements have been described in Cebulski & Pomeroy (2025b).

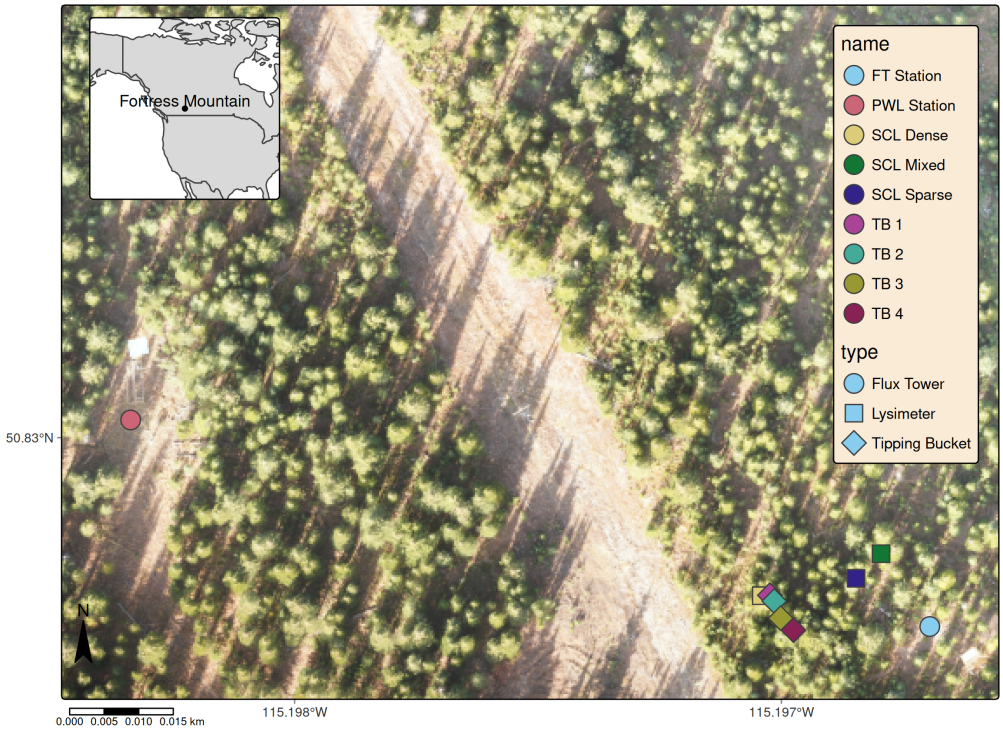

Figure 3: Map showing the location of flux towers and lysimeter instruments. The inset map on the upper left shows the regional location of Fortress Mountain Research basin. Flux towers are denoted by a circle, lysimeters by a square, and tipping bucket rain gauges (TB) by diamonds.

2.2 The Cold Regions Hydrological Model Platform

The Cold Regions Hydrological Model Platform (CRHM) was used to implement calculations of the canopy snow energy and mass budget. A full description of the CRHM platform is described in Pomeroy et al. (2022) and the source code is available at https://github.com/srlabUsask/crhmcode. The climate forcing data used to run CRHM was from station-based fifteen-minute interval measurements of air temperature, relative humidity, wind speed, precipitation, and incoming solar radiation from the FT, PWL, and FRS stations. CRHM incorporates a flexible modular design allowing the user to select various modules (parameterisations) that represent hydrological processes. The phase of atmospheric precipitation was determined from the energy balance of falling hydrometeors (Harder & Pomeroy, 2013). A new CRHM module was created here to simulate the coupled mass and energy balance of snow intercepted in the canopy. The energy balance is described in detail in Section 2.5 and the updates to the mass balance through revisions to the canopy snow unloading empirical functions are presented in Section 3.1.1 and Section 3.1.2.

2.3 Canopy Snow Mass Balance

The following mass balance as described in Cebulski & Pomeroy (2025a) was implemented in CRHM to track the state of canopy snow load (L, mm) over time:

$$\frac{dL}{dt} = [q_{sf} - q_{tf} + q_{ros}] - [q_{unld}^{melt} + q_{unld}^{dry}] - q_{drip} - q_{wind}^{veg} - q_{sub}^{veg} \tag{1}$$

where $\frac{dL}{dt}$ is the change in canopy snow load over time, (mm s^{-1}), q_{sf} is the snowfall rate (mm s^{-1}), q_{tf} is the throughfall rate (mm s^{-1}), q_{ros} is the rate of rainfall falling on snow intercepted in the canopy (mm s^{-1}), q_{unld}^{melt} is the unloading rate due to melt (mm s^{-1}), q_{unld}^{dry} is the dry snow unloading rate due to shear stress on snow, wind erosion, branch movement, structural degradation, bond weakening and increased elasticity of branches and other non-melt related processes (mm s^{-1}), q_{drip} is the canopy snow drip rate (mm s^{-1}) resulting from canopy snowmelt (q_{melt}, mm s^{-1}), q_{wind}^{veg} is the wind transport rate in or out of the control volume (mm s^{-1}), and q_{sub}^{veg} is the intercepted snow sublimation rate (mm s^{-1}) which includes any evaporation of liquid water in the canopy. Figure 1 in Cebulski & Pomeroy (2025a) presents a visual representation of this mass balance.

2.4 Mass Balance Parameterisations

In addition to the updated canopy snow model presented in this study, hereafter referred to as CP25 (described in Section 3.1.1 and Section 3.1.2), three other canopy snow models were implemented in CRHM following previous studies by Ellis et al.

(2010) and Floyd (2012) (E10), Roesch et al. (2001) (R01), and Andreadis et al. (2009) who built on observations by Storck et al. (2002) (SA09). The E10 model includes canopy snow sublimation as described in Pomeroy et al. (1998b), dry snow unloading as a function of canopy snow load from Hedstrom & Pomeroy (1998) with modifications described in Ellis et al. (2010) and Floyd (2012) to handle canopy snow melt and drip processes using an ice-bulb temperature threshold. The R01 model represents dry snow unloading, melt, and drip using linear functions of wind speed and air temperature, while sublimation is simulated using the parameterisation from Pomeroy et al. (1998b). The SA09 model unloads snow as a ratio of the canopy snowmelt rate, following observations by Storck et al. (2002) and does not include dry snow unloading. The snowmelt rate from Equation 3 was used to calculate the unloading rate for the Andreadis et al. (2009) unloading and thus differs from the energy balance routine described in their study. Canopy snow sublimation in SA09 was represented based on the Essery et al. (2003) parameterisation (Equation 10) as implemented in CP25.

The retention of canopy snow meltwater differs between the four canopy snow models implemented in CRHM. For E10, liquid meltwater is not retained in the canopy and immediately drips before it can evaporate. The R01 model also does not represent evaporation of liquid meltwater as canopy snow is not explicitly separated between solid snow unloading and melt/drip. The canopy liquid water storage capacity (L_{max}^{liq}, mm) from SA09 and CP25 was calculated as:

$$L_{max}^{liq} = Lh + nLAI \tag{2}$$

where h is the liquid meltwater holding capacity that canopy can retain against gravity and n is a storage constant of the vegetation elements. Andreadis et al. (2009) estimated h as 0.035 (-) and n as e^{-4}. In this study, h was set to 0.01 (-), and n was defined as $C_c \cdot 0.2$. A one-sided effective plant (leaf) area index (LAI) was used, including the clumping factor to account for needleleaf canopy structures, following the approach of Ellis et al. (2010) for rainfall interception.

2.5 Canopy Snow Energy Balance

The CP25 and SA09 canopy snow models implemented the following energy balance approach to calculate the energy available for melting snow intercepted in the canopy (Q_{melt}, W m^{-2}) and to track the canopy snow temperature over time ($\frac{\Delta T_{vs}}{\Delta t}$, K s^{-1}). The energy balance is expressed as:

$$Q_{melt} = Q_{sw} + Q_{lw} + Q_p + Q_h + Q_l - [C_p^{ice} L \frac{\Delta T_{vs}}{\Delta t}] \quad (3)$$

where Q_{sw} and Q_{lw} (W m^{-2}) are the net shortwave and longwave radiation heat fluxes to the canopy snow, Q_p (W m^{-2}), is the advective energy rate, and Q_l and Q_h (W m^{-2}), are the turbulent fluxes of latent heat and sensible heat respectively (positive towards canopy snow), and C_p^{ice} (J kg^{-1} K^{-1}) is the specific heat capacity of ice. Figure 2 in Cebulski & Pomeroy (2025a) shows a visual representation of this energy balance.

2.6 Energy Balance Parameterisations

The E10 and R01 parameterisations relied on physically guided empirical relationships to simulate sublimation and melt and are described in full detail in their respective articles and are also summarised in Cebulski & Pomeroy (2025a). The following section describes the energy balance parameterisations implemented in the CP25 and SA09 models.

Q_{sw} was determined as:

$$Q_{sw} = Q_{sw}^{in} \cdot (1 - \alpha_s) \cdot \tau_{50}^{veg} \quad (4)$$

where Q_{sw}^{in} is the downwelling shortwave radiation (W m^{-2}), α_s is the albedo of snow intercepted in the canopy (-), τ_{50}^{veg} (-) is the canopy transmittance to Q_{sw}^{in}. Equation 10 from Pomeroy et al. (2009) was used to determine τ_{50}^{veg}, using half of the leaf area index (LAI) based on studies Weiskittel et al. (2009) and Kesselring et al. (2024) that approximately 50% of the total leaf area is concentrated in the upper half of coniferous canopies. Q_{sw} provides an approximation of the net shortwave radiation to all snow intercepted in the canopy and is a simplification from using a partial differential equation to determine the radiation incident to individual height layers within the canopy. Upwelling shortwave radiation reflected off the surface snowpack is considered negligible contribution to the snow intercepted in the canopy as it is primarily blocked by vegetation elements underlying the canopy snow (Pomeroy et al., 2009).

Q_{lw} was approximated as:

$$Q_{lw} = \downarrow Q_{lw}^{atm} + \uparrow Q_{lw}^{veg} - Q_{lw}^{vs} \quad (5)$$

where Q_{lw}^{atm} is the downwelling longwave radiation from the atmosphere (W m^{-2}), Q_{lw}^{veg} is the longwave radiation upwelling from vegetation elements underlying snow intercepted in the canopy (W m^{-2}), and Q_{lw}^{vs} (W m^{-2}) is the outgoing longwave radiation from the top and bottom of the canopy snow layer calculated as:

$$Q_{lw}^{vs} = 2\epsilon_s \sigma T_{vs}^4 \tag{6}$$

where ϵ_s is the emissivity (-) of snow taken as 0.99 and σ is the Stefan–Boltzmann (5.67e^{-10} W m^{-1} K^{-4}). Q_{lw}^{atm} was approximated in this study as in Sicart et al. (2006) to represent the influence of atmospheric moisture and clouds on emissivity. Q_{lw}^{veg} was calculated with the assumption that canopy elements are in equilibrium with the air temperature plus any increase in vegetation temperature from the extinction of Q_{sw}^{in} in the canopy (Pomeroy et al., 2009, Eq. 4).

Q_p was calculated as:

$$Q_p = [C_p^{liq} m_r (T_r - T_{vs}) + C_p^{ice} m_s (T_s - T_{vs})]/\Delta t \tag{7}$$

where C_p^{liq} is the specific heat capacity of liquid water (J kg^{-1} K^{-1}), m_r is the specific mass of liquid water in precipitation (mm), T_r is the rainfall temperature (K), m_s is the specific mass of snow in precipitation (mm), and T_s is the snowfall temperature (K).

Q_h was calculated as:

$$Q_h = \frac{\rho_a}{r_a} C_p^{air} (T_a - T_{vs}) \tag{8}$$

where ρ_a is the air density (kg m^{-3}), C_p^{air} is the specific heat capacity of air (J kg^{-1} K^{-1}), T_a is the air temperature, and r_a is the aerodynamic resistance (s m^{-1}) which was approximated from Equation 4 in Allan et al. (1998) as:

$$r_a = \frac{\log(\frac{z_T - d_0}{z_0}) \log(\frac{z_u - d_0}{z_0})}{\kappa^2 u_z} \tag{9}$$

where z_T is the height of temperature measurement (m), d_0 is the displacement height (m) which was approximated as 2/3$^{\text{rd}}$ the mean canopy height, z_0 is the roughness length (m) which was approximated as 1/10$^{\text{th}}$ of the mean canopy height, z_u is the wind speed measurement height (m), κ is von Kármán's constant, 0.41 (-), and u_z is the wind speed measurement at z_u (m s^{-1}).

Q_l was calculated as:

$$Q_l = \frac{\rho_a}{r_i + r_a}(q_a(T_a) - q_{vs}(T_{vs})) \tag{10}$$

where r_i is a resistance for transport of moisture from intercepted snow to the canopy air space (Eq. 28 in Essery et al., 2003), $q_a(T_a)$ and $q_{vs}(T_{vs})$ are the specific humidity (-) at the air temperature and canopy snow temperature, respectively. r_i was calculated following the concept of how full the canopy is with snow as introduced by Pomeroy & Schmidt (1993) with modifications to incorporate a larger maximum canopy snow load capacity of 50 mm based on observations by Storck et al. (2002), Floyd (2012), and Cebulski & Pomeroy (2025b).

The above sensible and latent heat flux equations assume neutral atmospheric stability conditions, which is supported by the uncertainty of stability correction in forest canopies (Conway et al., 2018) and mountain environments in winter (Helgason & Pomeroy, 2012a). Solving Equation 3 requires an iterative solution to determine ΔT_{vs} and the remaining terms which are also a function of T_{vs}.

2.7 Influence of Predictive Variables on Unloading

The effects of air temperature, wind speed, snow load, melt, and sublimation on the unloading process were assessed using a multivariate ordinary least squares regression. The following hypotheses were tested:

a. Melt promotes unloading through loss of structural integrity, particle bond weakening, and lubrication of intercepted snow.
b. Sublimation promotes unloading via structural degradation and bond weakening of intercepted snow.
c. Wind drag promotes unloading through shear stress applied to intercepted snow, wind erosion through direct entrainment in the atmosphere of intercepted snow, and branch movement.
d. Increasing air temperature promotes unloading by increasing the elasticity of branches and its association with melt and/or sublimation.

Since these processes occur simultaneously and could not be isolated experimentally, different combinations of the independent variables were included in the regression to identify which sets of processes significantly influenced unloading. The subcanopy lysimeter unloading measurements had a high relative instrument error due to the relatively small accumulation of unloaded snow over the 15-min intervals. To improve instrument accuracy, whilst maintaining consistency of the unloading measure-

ments with the independent variables, the 15-min interval measurements of unloading were aggregated over differing predictive variable bins. Independent variable bins that had less than 0.1 mm of accumulated snow were removed, resulting in a mean instrument error of +/- 2% for the remaining bins. Air temperature and wind speed were measured at the FT station, canopy snow load from the weighed tree lysimeter (scaled to the canopy of each respective subcanopy lysimeter), and canopy snowmelt and sublimation simulated using CRHM with the CP25 model as described in the previous section. The individual processes found to be significant predictors of unloading in the multivariate regression (i.e., shear stress and canopy snow melt) were isolated to parameterise a model of their effects that was implemented in the CP25 model.

2.7.1 Dry Snow Unloading

Wind, shear stress, and canopy snow load were assessed as predictors of dry snow unloading during intervals without canopy snowmelt. These periods were defined using simulated canopy snowmelt in CRHM as well as visual analysis of time-lapse imagery for canopy snow drip and/or icicle formation. The relationships between wind speed, shear stress, canopy snow load, and unloading were analyzed using linear and non-linear least squares regressions, linearly with shear stress and exponentially with wind speed. The linear relationship between shear stress, canopy load, and unloading did not include an intercept term and was thus the coefficient of determination (R^2) was adjusted following (Kozak & Kozak, 1995).

2.7.2 Canopy Snowmelt Induced Unloading

A mass balance approach was incorporated to determine the unloading rate resulting from canopy snowmelt (q_{unld}^{melt}, mm s^{-1}). The effect of the canopy snowmelt rate (q_{melt}) on unloading was then assessed by fitting a linear model using an ordinary least squares regression. Since direct measurements of canopy snow unloading are challenging to obtain independently from canopy snowmelt drainage (Storck et al., 2002), the mass balance introduced in Equation 1 was incorporated to determine q_{unld}^{melt} as a residual. During intervals without $[q_{sf} - q_{tf} + q_{ros}]$ or q_{wind}^{veg} Equation 1 was simplified and rearranged to:

$$q_{unld}^{melt} = -\frac{dL}{dt} - q_{drip} - q_{unld}^{dry} - q_{sub}^{veg} \tag{11}$$

While some components of the canopy snow mass balance can be measured directly, such as $\frac{\Delta L}{\Delta t}$ with the weighed tree, sublimation of canopy snow is more difficult to quantify directly especially in forested mountain environments (Conway et al., 2018;

Harding & Pomeroy, 1996; Helgason & Pomeroy, 2012b; Parviainen & Pomeroy, 2000) and thus q_{sub}^{veg} was simulated in this study in CRHM using Equation 10 as described in Essery et al. (2003). q_{drip} was measured where possible using the rain gauges, however problems with freezing of liquid water in the tipping bucket mechanisms limited the ability to measure q_{drip} reliably. Thus, q_{drip} was also estimated using simulations of canopy snowmelt (q_{melt}) in CRHM as in Equation 3, with storage limited by the canopy liquid water holding capacity and drainage of excess water. Canopy snow ablation periods that were dominated by melt were selected for calculating q_{unld}^{melt} where the contribution of q_{unld}^{dry} and q_{sub}^{veg} to canopy snow ablation was less than 5%.

3 Results

3.1 Unloading Relationships

Amongst the models evaluated, a multivariate linear regression incorporating canopy snow load, canopy snowmelt, and wind speed provided the highest explanatory power for predicting canopy snow unloading measured by subcanopy lysimeters ($R^2 = 0.79$, p < 0.05; Table 1). Shear stress was found to explain less variability compared to wind speed, when both were combined with canopy snow load and snowmelt ($R^2 = 0.71$, $p < 0.05$). Air temperature and canopy snow sublimation were not significant predictors in any model ($p > 0.05$; Table 1). A model including only canopy load, air temperature, and wind speed produced an R^2 of 0.11 however, only canopy load and wind speed were statistically significant ($p < 0.05$). As shown in Figure 4, unloading rates varied more with snowmelt and sublimation (0–2 mm hr^{-1}) than with air temperature and wind speed (0–0.5 mm hr^{-1}).

The mean unloading rate was observed to increase with increasing canopy load, air temperature, ice-bulb temperature depression, shear stress, and wind speed (Figure 4). An increase in unloading was found with sublimation rates between 0—0.3 mm hr^{-1} (Figure 4). For sublimation rates higher than 0.3 mm hr^{-1}, unloading declined with sublimation. The decline in unloading with wind speed >3 m s^{-1} might have been contributed to by wind transport and entrainment into the atmosphere, and/or increased sublimation rates at higher wind speeds.

Table 1: Summary of multivariate linear regression results evaluating all combinations of predictor variables for canopy snow unloading including: canopy load (L), wind speed (u), canopy snowmelt rate (q_{melt}), canopy snow sublimation rate (q_{subl}), and air temperature (T_a). Columns L to T_a show the coefficient estimate for each respective term, and the significance of each term is shown in brackets. Significance codes: * = p < 0.05; ns = not significant (p > 0.05). The models are ranked by their corresponding AIC value.

Model Name	Intercept	L	u	q_{melt}	q_{subl}	τ	T_a	R^2	AIC
M1	-0.11 (ns)	0.02 (*)	0.08 (*)	0.40 (*)	—	—	—	0.79	-12.8
M4	-0.08 (ns)	0.04 (*)	—	0.39 (*)	—	0.75 (*)	—	0.71	5.5
M7	0.13 (ns)	0.02 (*)	—	0.32 (*)	-0.22 (ns)	—	—	0.54	10.0
M10	-0.06 (ns)	0.02 (*)	0.08 (*)	0.38 (*)	—	—	0.00 (ns)	0.52	-4.4
M24	-0.00 (ns)	0.02 (*)	0.05 (*)	0.36 (*)	0.13 (ns)	—	—	0.37	-2.0
M40	0.07 (ns)	0.01 (*)	0.06 (*)	—	—	—	0.01 (ns)	0.11	2.4
M63	0.22 (*)	0.00 (ns)	-0.01 (ns)	—	0.07 (ns)	—	—	- 0.02	39.8

3.1.1 The Influence of Wind on Dry Snow Unloading

Canopy snow unloading measured from the subcanopy lysimeters—filtered to include intervals without canopy snowmelt—were positively associated in a linear relationship with shear stress and an exponential relationship with wind speed (Figure 5). The following equations were fitted to these relationships and tested.

The dry unloading rate, q_{unld}^{dry}, was represented as a linear function of shear stress:

$$q_{unld}^{dry} = L \cdot \tau_{mid} \cdot a \tag{12}$$

where τ_{mid} is the shear stress at mid canopy height and a is a fitting constant.

An exponential function of wind speed was defined as:

$$q_{unld}^{dry} = L \cdot u_{mid} \cdot a \cdot e^{b \cdot u_{mid}} \tag{13}$$

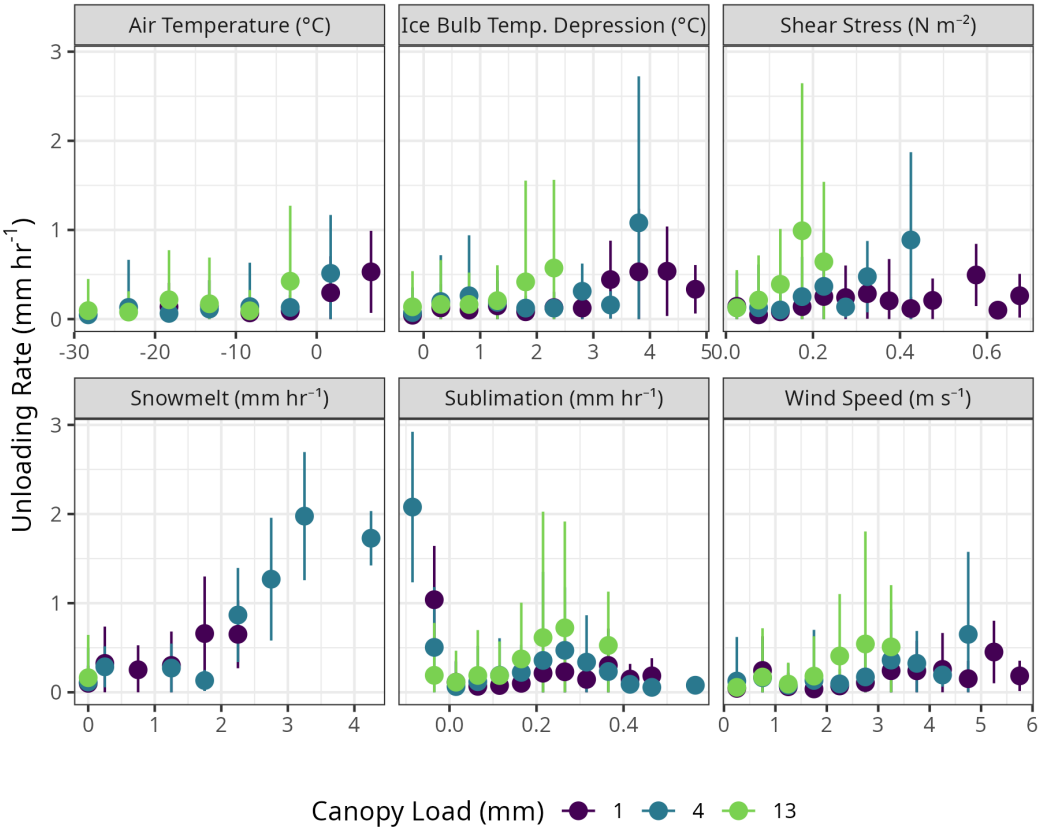

Figure 4: Scatter plots showing the mean unloading rate (mm hr^{-1}) for differing bins of air temperature (°C), ice-bulb temperature depression (°C), shear stress (N m^{-2}), canopy snowmelt (mm hr^{-1}), canopy snow sublimation (mm hr^{-1}), and wind speed (m s^{-1}). Note: unloading was measured by the subcanopy lysimeters, air temperature and wind speed were measured at FT station, canopy snowmelt and sublimation were calculated using CRHM.

where u_{mid} is the wind speed at mid canopy height, and a and b are fitting constants.

The shear stress relationship (Equation 12) accounted for slightly more variability in unloading ($p < 0.05$, $R^2 = 0.61$) compared to wind speed ($p < 0.05$, $R^2 = 0.54$) (Table 2). The mean bias of the shear stress model of 0.037 mm hr^{-1} was also lower compared to the wind speed model of 0.048 mm hr^{-1}, additional model error statistics and fitting coefficients are provided in Table 2. Both models exhibited considerable scatter, with notable uncertainty resulting from instrument error and processes other than wind contributing to unloading (Figure 5). The wind-induced unloading rate was observed to be higher for greater canopy snow loads (Figure 5). The R^2 of both the shear stress and wind speed relationships was much higher than the variance explained by wind speed when including intervals with melting snow (Table 1). The higher R^2 of the shear stress model compared to wind speed, coupled with the better physical representation of kinetic energy, suggests that shear stress be selected as the independent variable to predict dry snow unloading in the model evaluation.

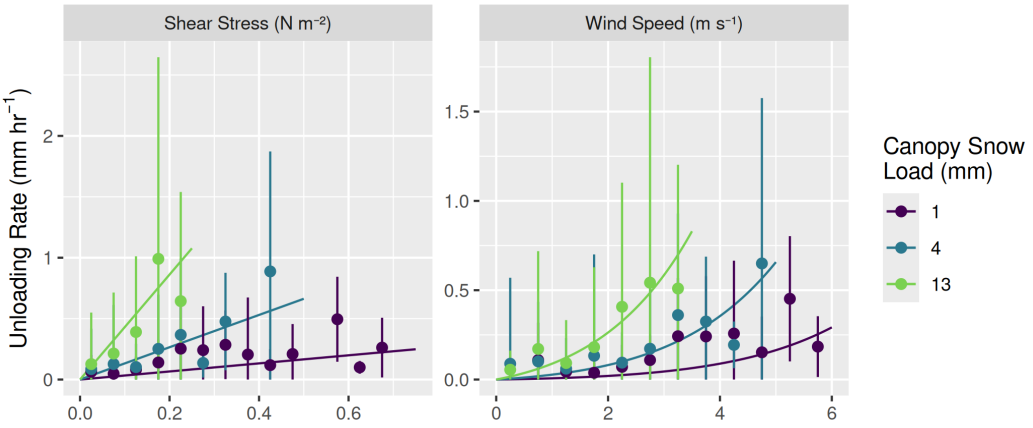

Figure 5: Canopy snow unloading rate measured by the subcanopy lysimeters versus shear stress (left) and wind speed (right) during periods without canopy snowmelt. The dots represent mean unloading rates within bins of shear stress and wind speed for three canopy snow load levels; error bars indicate +/- 1 standard deviation. The fitted lines show predictions from Equation 12 (left) and Equation 13 (right).

Table 2: Summary of regression error statistics and coefficients for the relationship between canopy snow unloading with wind speed (Equation 12) and shear stress (Equation 13), as shown in Figure 5. Coefficients are shown for hourly unloading.

Metric	Wind	Shear Stress
Mean Bias (mm/hr)	0.048	0.037
Mean Absolute Error (mm/hr)	0.087	0.115
Root Mean Square Error (mm/hr)	0.11	0.15
Coefficient of Determination (R^2)	0.54	0.61
Coefficient a	4.62×10^{-03}	3.31×10^{-01}
Significance of a	$p < 0.05$	$p < 0.05$
Coefficient b	3.93×10^{-01}	NA
Significance of b	$p < 0.05$	NA

3.1.2 The Influence of Melt on Unloading

Five warm & humid events were selected, in which the median air temperature was above 0°C and relative humidity was above 65%, resulting in less than 5% contribution of dry snow unloading and sublimation to ablation as determined by the CP25 model. For these events, unloading was calculated using Equation 11 and canopy snowmelt rates were calculated using CRHM with Equation 3. These unloading estimates were found to be positively correlated with canopy snowmelt (Figure 6).

When canopy snow loads remained between 0 and 5 mm, the unloading-to-melt ratio varied from approximately 0 to 0.5. As snow loads increased, this ratio increased linearly, reaching its peak value of 5.0 for a canopy snow load of 30 mm (Figure 6). This relationship can be expressed through a linear function:

$$q_{unld}^{melt} = R \cdot q_{melt}(L) \tag{14}$$

where R represents the unloading-to-snowmelt ratio and q_{melt} is the canopy snowmelt rate (mm hr^{-1}). Equation 14 is similar to Equation 33 in Andreadis et al. (2009); however, instead of a constant value of 0.4 for R, it was determined as:

$$R = m \cdot L + b \tag{15}$$

where m and b were determined as 0.16 and -0.5, respectively, using an ordinary least squares regression. Equation 14 using these fitted parameters resulted in a

statistically significant relationship ($p < 0.05$, $R^2 = 0.73$) (Figure 6). Additional observations of canopy snowmelt from the subcanopy rain gauges were also used to estimate R (Figure 6). The number of usable observations was limited to three events (out of the 5 warm & humid events) due to freeze-thaw events that seized up the tipping bucket mechanisms in the rain gauges, however, these measurements are still useful in providing some validation of the CRHM canopy snowmelt/drip calculations (Figure 7). The CRHM-estimated cumulative drip was higher than the subcanopy rain gauges for two out of the three melt events. Differences in the timing and magnitude of the observed and simulated values were expected due to both instrument uncertainties in the rain gauges from freezing of rain gauges and thawing of snow in the collection funnels, and in the canopy snow energy balance simulation.

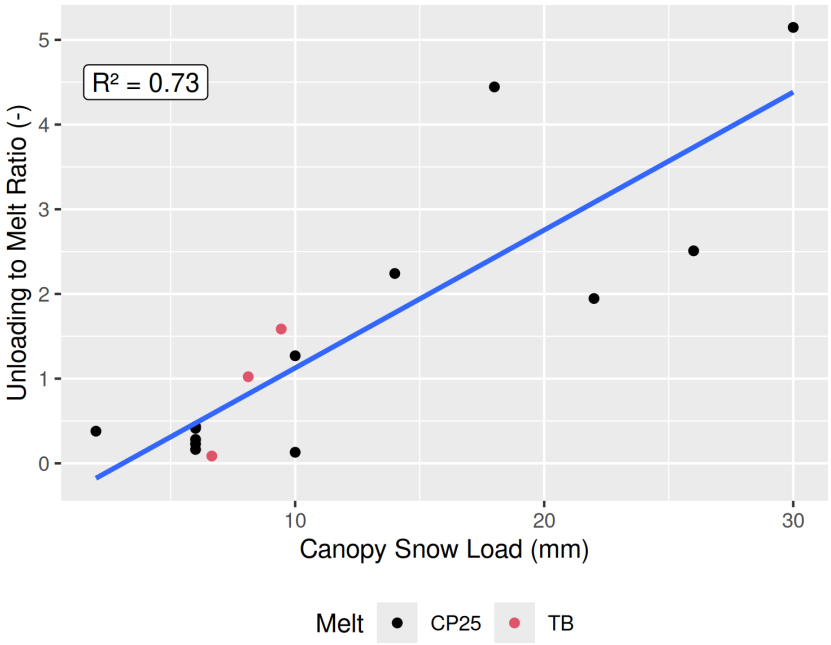

Figure 6: The ratio of canopy snow unloading (weighed tree residual) to snowmelt across different canopy snow load bins and events. Black dots represent the observed cumulative unloading divided by the cumulative simulated snowmelt from the updated CP25 canopy snow routine in CRHM for each of the five warm & humid events. Red dots show the cumulative observed unloading divided by snowmelt measured by the rain gauges. Multiple dots within a bin correspond to different events. The blue line represents the best-fit line derived from ordinary least squares regression.

3.2 New Canopy Snow Model

The CP25 model is based on the canopy snow mass balance formulation (Equation 1), where q_{tf} was represented as:

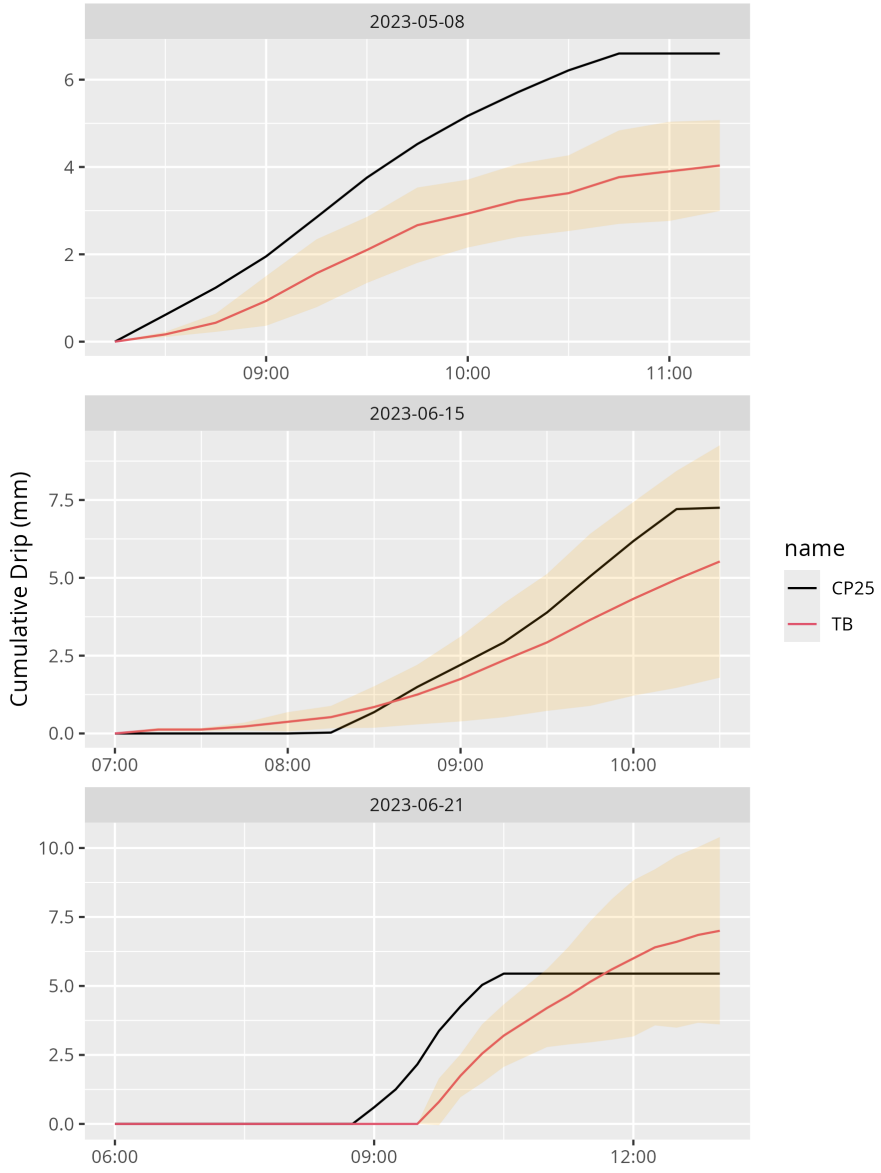

Figure 7: Cumulative canopy snow drip measured by the average of four subcanopy tipping bucket rain gauges (TB) and simulated using the CRHM CP25 model (Equation 3). Yellow shading indicates the range of ±1 standard deviation amongst the individual rain gauge measurements.

$$q_{tf} = [(1 - C_p)\alpha]q_{sf} \tag{16}$$

where C_p is the leaf contact area calculated using Equation 10 in Cebulski & Pomeroy (2025b) and α is an efficiency constant. Melt-driven unloading (q_{unld}^{melt}) was modelled using Equation 14, while dry snow unloading (q_{unld}^{dry}) was represented using Equation 12. Canopy snow drip (q_{drip}) is derived from calculations of canopy snowmelt from Equation 3, with storage limited by the canopy liquid water holding capacity computed from Equation 2; any excess was assumed to immediately drain. Wind transport of canopy snow (q_{wind}^{veg}) is incorporated in the Equation 12 calculation. Sublimation of intercepted snow (q_{veg}^{sub}) was represented using Equation 10.

3.3 Event-based Evaluation of Canopy Snow Ablation Models

The updated canopy snow model (CP25), as well as the existing models R01, SA09, and E10 were evaluated using weighed tree lysimeter measurements of canopy load during seventeen canopy snow ablation events. The seventeen ablation events had air temperatures ranging from -30.5°C to +6.9°C and wind speeds from calm to 5.3 m s^{-1} (Figure 8). This range of meteorological conditions is particularly wide and spans conditions typical of the cold boreal to temperate maritime needleleaf forests. Events were classified as cold & dry, cold & humid, warm & dry, and warm & humid based on the median event air temperature (above or below 0°C) and relative humidity (above or below 65%) (Figure 8).

Simulated canopy snow load by the CP25 model closely matched the observations for all 17 events, demonstrating the most consistent agreement amongst the models evaluated (Figure 9). The large declines in canopy snow load for E10 (Figure 9) are due to the maximum canopy snow load used in this model which ranged from 7 to 12 mm depending on the fresh snow density (a function of air temperature in Hedstrom & Pomeroy, 1998).

The energy balance-based snowmelt modelling approaches (CP25 & SA09) yielded the most accurate representation of canopy snowmelt over the warm & humid events. The CP25 mean bias of 0.02 mm hr^{-1}, which was smaller than the -0.11 mm hr^{-1} bias associated with SA09 (Figure 10). The improvement for CP25 over SA09 comes from its representation of the increase in unloading at higher canopy snow loads (Figure 6), as observed for the 2022-06-14 event (Figure 9). The air temperature (R01) and ice-bulb temperature (E10) models produced a wider range of mean biases (Figure 10) and larger mean bias of over 0.42 mm hr^{-1} during the warm & humid events, compared to CP25 and SA09. The rate of ablation was slower for canopy

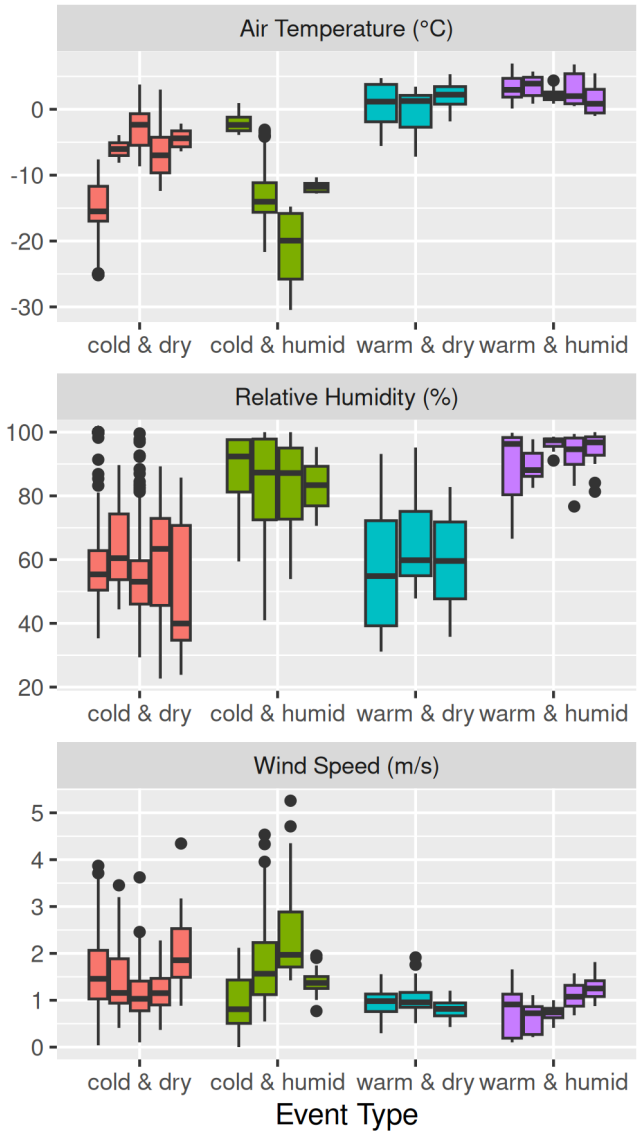

Figure 8: Boxplots showing the distribution of meteorological measurements of air temperature, relative humidity, and wind speed over each of the seventeen select ablation events. Air temperature, relative humidity, and wind speed were measured at FT station. Note: the rectangle vertical extent represents the interquartile range (25^{th} to 75^{th} percentile), the horizontal line within each box indicates the median, and the whiskers extend to 1.5 times the interquartile range. Circular points beyond the whiskers represent outliers.

snow loads below ~1.5 mm and ~0.3 mm for CP25 and SA09 respectively; due to their differing liquid water storage capacities (Figure 9). For the warm events other than 2022-04-23, the observed decline in ablation rate occurs around 2 to 3 mm, exceeding the threshold predicted by all models.

The warm & dry events had consistent performance with mean biases of 0.02 mm hr^{-1} for each of the four models (Figure 10). Initiation of ablation was delayed compared to observations from the weighed tree for the CP25 and SA09 models for all three of the warm & dry events (Figure 9). The temperature threshold methods (E10 & R01) achieved better timing on the onset of ablation for two events (2022-03-29 and 2022-04-21) compared to CP25. However, E10 initiated the onset of ablation slightly earlier for 2022-04-23 and the rate of ablation was also lower than observed for this event.

For the cold & dry events, all models had accurate performance with mean biases ranging from -0.01 to 0.01 mm hr^{-1}, with a slight improvement in the mean bias for CP25 of -0.009 mm hr^{-1} (Figure 10). Canopy snowmelt was overestimated by the E10 model and caused the steep initial decline in canopy snow load on 2022-03-02 which is not registered by the weighed tree or other models. However, underestimates of ablation compensated for this overestimate over the remaining cold & dry events—which had moderate wind speeds—as wind-driven unloading is not included in the E10 model (Figure 8). For events 2022-03-02 and 2023-03-14 the R01 model overestimated canopy snow ablation due to an overestimation of wind-driven unloading (Figure 9).

The importance of representing wind-driven unloading was clear during the cold & humid events, where the mean bias of models including this mechanism was reduced compared to other approaches; for example, 0.04 mm hr^{-1} for R01 and 0.15 mm hr^{-1} for CP25. In contrast, simulations that did not explicitly account for wind-driven unloading exhibited higher biases, exceeding 0.32 mm hr^{-1} (Figure 10). Although the E10 model does not include wind-driven unloading, it performed best for the 2023-02-26 event due to its relatively slow time-based unloading rate compared to CP25 and R01 which overestimate ablation for this event (Figure 9). The R01 model overestimated unloading over most of the cold & humid events and had a higher median bias for the cold & humid events compared to CP25 (Figure 10). The CP25 model had consistently lower bias across the three cold & humid events, but still underestimated ablation for the 2023-02-24 event which had peak wind speeds of over 5 m s^{-1}. Over this event, 1.3 mm of snow was measured at a shielded precipitation gauge in a nearby clearing and was likely derived from wind transport of snow

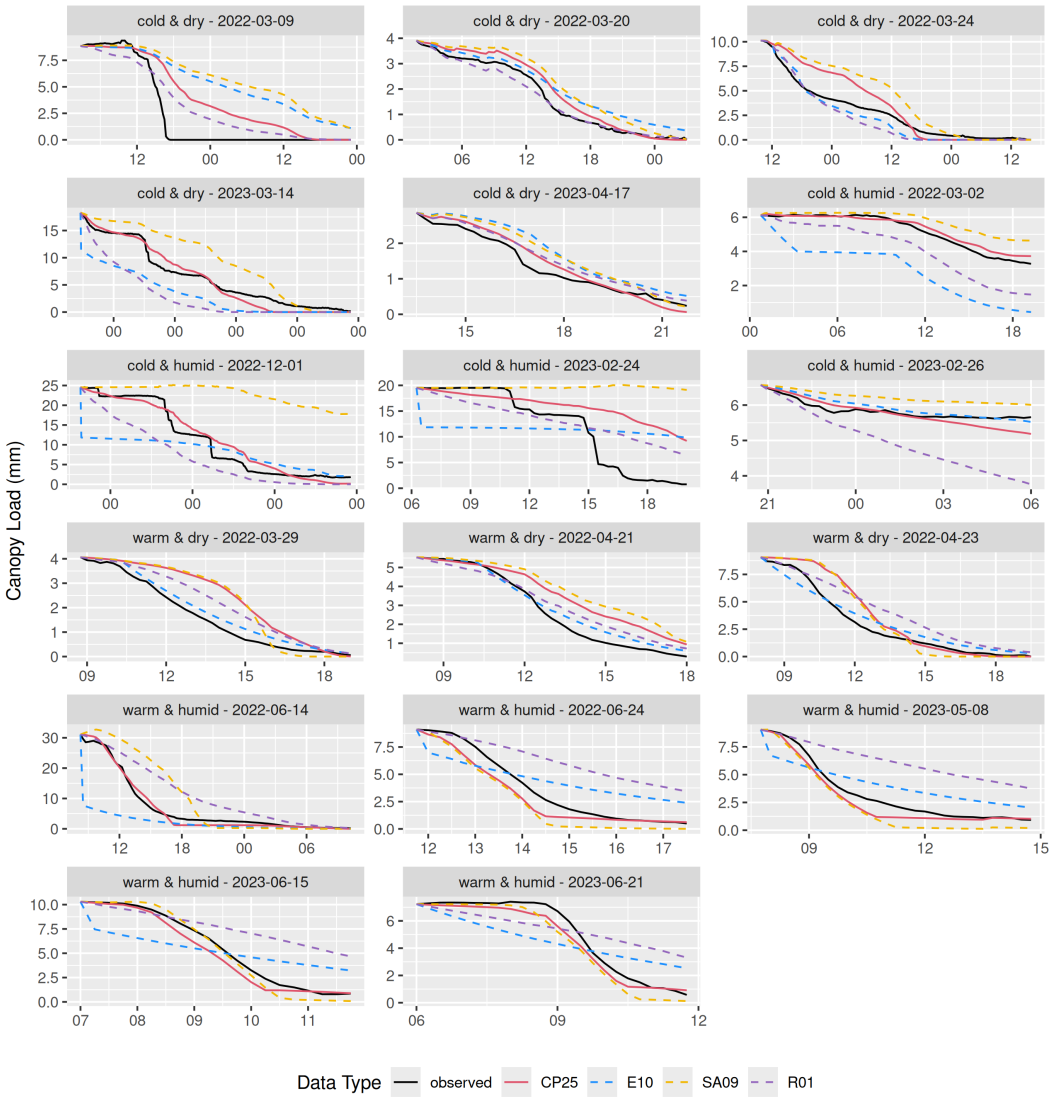

Figure 9: Time series of canopy snow load for individual events measured by the weighed tree (observed) and simulated using the four canopy snow models.

from the canopy, as clear skies with no precipitation were observed. The amount of snow observed to unload from the canopy into the subcanopy lysimeters during this event was consistent with simulated unloading in CRHM suggesting that the remaining unaccounted-for snow was likely entrained into the atmosphere and sublimated and/or transported to distant sites.

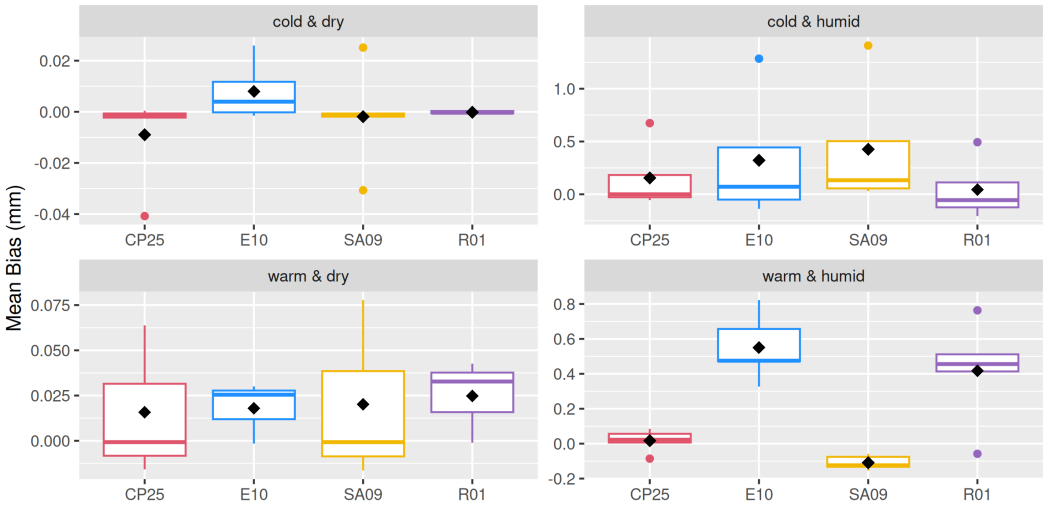

Figure 10: Boxplots illustrating the distribution of event mean biases calculated between simulations of canopy snowload and observations from the weighed tree. The vertical extent of each rectangle represents the interquartile range (25^{th} to 75^{th} percentile), the horizontal line within each box indicates the median, and the whiskers extend to 1.5 times the interquartile range. Circular points beyond the whiskers represent outliers. The diamonds represent the mean of the event biases.

3.4 Canopy Snow Partitioning

During warm & humid events, all four parameterisations showed relatively consistent partitioning of canopy snow, with only a small fraction returned to the atmosphere (Figure 11). The warm & dry events had greater variability in the partitioning of intercepted snow—when compared to the warm & humid events—with a larger contribution from sublimation and evaporation processes. Increased unloading from the E10 model resulted in a greater fraction of intercepted snow reaching the ground compared to the CP25 model over the warm & dry events.

For the cold & dry and cold & humid events, the two parameterisations that include wind-driven unloading (R01 and CP25) had differing fractions of snow partitioned to the ground via unloading. A higher fraction of intercepted snow reached the ground for R01 due to the higher dry snow unloading rate compared to CP25 over all of the cold events. For both the cold & dry and cold & humid events SA09 partitioned all

snow back to the atmosphere via sublimation as dry snow unloading is not included in this parameterisation. Although CP25 and E10 include differing unloading processes, when averaged over all events, both had a similar fraction of snow reaching the ground (70%) versus the atmosphere (30%) (Table 3). SA09 has the largest discrepancy which returned 40% of intercepted snow back to the atmosphere and the R01 with the least amount of snow reaching the atmosphere with 24%.

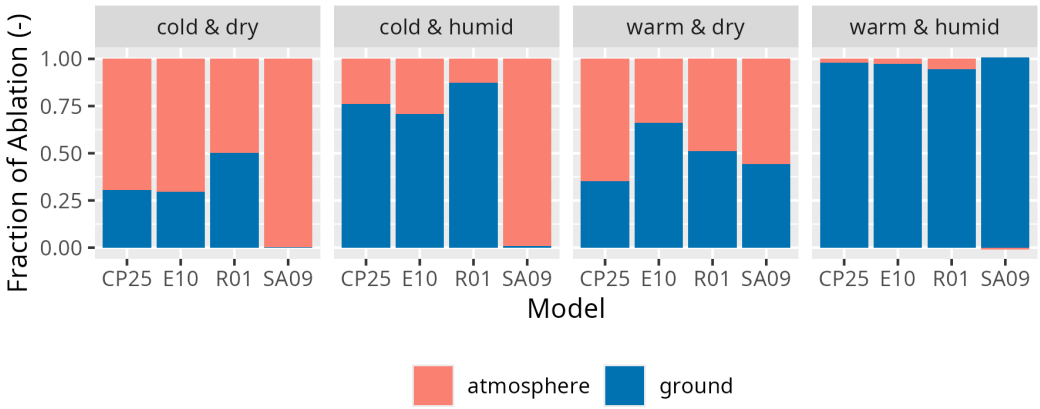

Figure 11: Bar chart illustrating the proportion of intercepted snow that was either lost to the atmosphere as sublimation and/or evaporation of melted snow or transferred to the ground through unloading or drip of melted snow by each event type for all 17 events.

Table 3: Fraction of canopy-intercepted snow returned to the atmosphere as sublimation and evaporation of melted snow or input to the ground as unloading or drip of melted snow for each parameterisation over the 17 select ablation events.

Model	Atmosphere (-)	Ground (-)
CP25	0.29	0.71
E10	0.31	0.69
R01	0.24	0.76
SA09	0.40	0.60

4 Discussion

4.1 Processes Governing Canopy Snow Unloading

Observations of canopy snow unloading support the hypothesis that unloading is primarily controlled by snowmelt and dry-snow related processes, both of which are also influenced by the amount of snow intercepted in the canopy (Table 1). The ratio of unloading to canopy snowmelt was found to increase linearly with increasing

canopy snow load (Figure 6), which differs from Storck et al. (2002) who originally found the ratio of canopy snow unloading to melt to be constant at 0.4. The measurement difficulties noted by Storck et al. (2002) limited their estimate of this ratio to a single mid-December event, preventing any association with canopy snow load. Similar instrument difficulties here in measuring canopy snowmelt drainage limited direct measurements to three events and hybrid measurements (from Equation 11) to 5 events (Figure 6). The reasonable correspondence between observed and modelled canopy snow drip for these events supports the linear increase hypothesis (Figure 7). Previous studies have identified relationships between melt-induced unloading and various meteorological parameters, including empirical functions of air temperature (Katsushima et al., 2023; Roesch et al., 2001), ice-bulb temperature (Ellis et al., 2010; Floyd, 2012), and solar radiation (Katsushima et al., 2023). Although branch bending and subsequent unloading has been shown to be associated with air temperature (Schmidt & Gluns, 1991; Schmidt & Pomeroy, 1990), observations here indicate that temperature-related unloading increases occur primarily near the freezing point (Figure 4), eliminating the need for a separate temperature parameterisation beyond snowmelt-associated unloading processes.

Dry snow unloading was found to increase exponentially with wind speed and linearly with shear stress (Table 2). These results differ from earlier research that has represented this process as a linear function of wind speed and canopy load (Bartlett & Verseghy, 2015; Katsushima et al., 2023; Roesch et al., 2001), as shown in Figure 1. The higher R^2 found for shear stress compared to wind speed for predicting unloading—when excluding melt events—is likely due to the physical relationship between shear stress force and kinetic energy transfer to the canopy, wind transport from the canopy, and movement of branches in the canopy induced by drag (shear) forces. The differing relationship presented here, compared to the R01 model (Figure 1), may be attributed to the development of that parameterisation using above canopy albedo as a proxy for canopy snow unloading (Bartlett & Verseghy, 2015; Roesch et al., 2001). This approach would have included both unloading and sublimation processes, in addition to greater measurement uncertainties (Cebulski & Pomeroy, 2025a). Conversely, the subcanopy lysimeter measurements employed here provided a more direct quantification of canopy snow unloading rates. Simulated unloading over events classified as cold & humid—which had the largest contribution of wind-driven unloading—resulted in the highest overall mean biases compared to the warm & dry, warm & humid, and cold & dry events (Figure 10). Additional factors that may influence dry snow unloading that are not considered in the new parameterisation (Equation 13) include wind erosion, branch movement, structural

degradation, bond weakening, increased elasticity of branches, snow density, and liquid water content. The addition of liquid water content in the canopy snow due to phase change can increase cohesion and adhesion of snow clumps within the canopy (Pomeroy & Gray, 1995). However, high liquid water contents during rapid melt can lubricate the snow attachment to the canopy and weaken cohesive bonds, inducing unloading, much as for wet snow avalanches (Baggi & Schweizer, 2008).

The density of snow intercepted in the canopy is expected to influence both dry snow and melt-induced unloading processes—and is incorporated in the E10 parameterisation for the initial accumulation component based on the findings of Schmidt & Gluns (1991)—but is not explicitly represented in any of the ablation calculations included in this study. Fresh, low-density snow typically exhibits lower cohesion and adhesion compared to older snow, which may have undergone freeze-thaw cycles or equitemperature metamorphism, processes that increase snow density and bond strength hence, increasing the mechanical resistance to unloading. While vapour deposition and rime-ice accumulation are simulated in some models (e.g., Clark et al., 2015; Ellis et al., 2010) via the latent heat flux parameterisation, they are usually treated as additions to the canopy snow reservoir. However, in humid or maritime regions rime can form dense, ice-like structures (e.g., Berndt & Fowler, 1969) with high resistance to unloading by either melt or wind (Lumbrazo et al., 2022). Although canopy snow density is expected to influence ablation processes, it was not observed in this study due to its continental location and remains a research gap for maritime climates.

The relationship between unloading and canopy snow sublimation was not statistically significant (Figure 4). This differs from earlier work by MacDonald (2010) who found an association between these two variables and attributed this to the reduction in structural integrity and bond weakening of the canopy snow clumps as snow particles are removed through sublimation. It is possible that the association identified by MacDonald (2010) arose from the concurrent increase in canopy energy inputs that promote both sublimation and other ablation mechanisms such as melt and other dry snow unloading processes which were not directly accounted for.

4.2 Performance Comparison of Ablation Models

The improved performance of the new CP25 model across a wide range of meteorological conditions demonstrates the advantages of incorporating comprehensive snow unloading processes coupled with physically based representations of the energy balance to simulate ablation (Figure 9). In contrast, existing models were limited by missing processes such as wind-driven unloading (SA09 and E10) or relied on

temperature-dependent parameterisations of melt and drip processes which had limited transferability across differing events (R01 and E10). Although the SA09 model—originally developed in a relatively warm maritime climate with limited wind influence (Storck et al., 2002)—performed similarly well to CP25 during most of the melt-dominated events, its exclusion of wind-induced unloading led to poor performance for the cold & dry and cold & humid events. This process omission caused SA09 to overestimate sublimation when averaged over all events (Table 3). Moreover, the constant canopy snow unloading to melt ratio of 0.4 in the SA09 model led to reduced performance for one melt event with canopy snow loads up to 30 mm, whereas the CP25 model more accurately predicted ablation over this event. The low liquid water retention capacity implemented in SA09 also contributed to an underestimation of canopy loads during the end of most melt events (Figure 9).

Models utilising temperature-based canopy snowmelt parameterisations (E10 and R01) exhibited inconsistent performance, particularly during warm & humid events where they underestimated ablation. This was due to their reliance on air temperature or ice-bulb temperature as proxies for energy input into the canopy, which failed to represent the energy availability over these events. In contrast, all four models performed similarly during warm & dry events, where air temperatures were closer to 0°C. The superior performance of the energy balance-based canopy snowmelt models (CP25 and SA09) during warm & humid events likely reflects their ability to represent the elevated energy inputs which were present over the warmer events.

While E10 omitted any explicit representation of wind-driven unloading, its exponential time decay parameterisation indirectly addressed this process, though it still underestimated overall ablation for the cold events which had higher wind speeds (Figure 9). The maximum canopy snow load threshold implemented in the E10 model was lower than observations from the weighed tree. This limitation offset its tendency to underestimate unloading processes as was also observed by Lundquist et al. (2021) and Lumbrazo et al. (2022). In this study, the CP25, SA09, and R01 models did not include a maximum snow load, and their performance aligns with the hypothesis of Lundquist et al. (2021) that this limit may be unnecessary—or much higher than previously though—when combined with a comprehensive canopy snow ablation routine. In contrast, R01 consistently overestimated wind-driven unloading during both the cold & dry and cold & humid events, potentially due to the differing methodology used to develop this parameterisation (Figure 9). CP25 provided a better representation of wind-driven unloading compared to R01 aside

from one one event with high wind speeds (>5 m s^{-1})—that cause wind redistribution/entrainment of snow into the atmosphere. Wind unloading parameters also may be influenced by tree species, forest structure, and snow characteristics (Lumbrazo et al., 2022), necessitating further field-based research on canopy snow unloading in diverse environments to assess their broader applicability.

The infrequent occurrence of wind-transport from the canopy in our observations may account for underestimation of ablation during one strongly wind-dominated events by CP25 (2023-02-24, Figure 9). Wind transport of canopy snow to the nearby Powerline snowfall gauge occurred during this event, but was a small fraction of canopy snow ablation, 1.3 mm of a total of 20 mm of canopy snow ablation. Since unloading measured by the subcanopy lysimeters corresponded well with CP25 predictions for this event, the approximately 9 mm of unaccounted canopy snow ablation may be attributed to uncertainties within the wind-driven unloading parameterisation (Figure 5) and possible atmospheric entrainment of canopy snow that was either transported to distant locations and/or sublimated. These findings align with observations by Troendle (1983) but contrast with Hoover & Leaf (1967), who proposed that most wind-transported snow relocates to nearby sites with minimal sublimation effects.

4.3 Canopy Snow Partitioning

Substantial variability was found in the fraction of snow that sublimated and/or evaporated as liquid meltwater versus unloading and drip depending on the canopy snow ablation model selected (Figure 11). For example, the exclusion of wind-driven unloading processes in the SA09 model resulted in 100% of intercepted snow reaching the atmosphere for both the cold & dry and cold & humid events. This differed considerably from the CP25 model which returned 70% and 24% of snow back to the atmosphere for the cold & dry and cold & humid events, respectively. Although E10 and CP25 include differing process representations, they predicted comparable fractions of snow reaching the ground versus returning to the atmosphere. The agreement between CP25 and E10 is notable, since the E10 has been tested and found to perform well in predicting subcanopy snowpacks around the world (Ellis et al., 2010; Gelfan et al., 2004; Pomeroy et al., 2022; Sanmiguel-Vallelado et al., 2022). However, the results shown here reveal that E10's individual process representations can be in error, particularly under warm and windy conditions, potentially explaining the difficulties when applying E10 at locations where parameterisation errors fail to offset one another (Lumbrazo et al., 2022; Lundquist et al., 2021). For example, at locations which intercept a larger amount of snow, the E10 maximum canopy

snow load would overestimate the amount of unloading, and a greater deviation between the E10 and CP25 model is expected.

4.4 Future Directions

Physically based approaches such as CP25 are particularly relevant for predictions of snow hydrology under a changing climate, where warming may reduce the reliability of empirically derived canopy snowmelt models like E10 and R01. The improved representation of melt events by CP25 and SA09 demonstrates the reliability of more physically based methods across a range of meteorological conditions, compared to temperature-based canopy snowmelt routines (E10 and R01) which had reduced performance over these events. Amongst all canopy snow ablation processes, dry snow unloading introduced the most uncertainty. Although the revised model performed best for this dataset, further validation is required across a wider range of climates and forest structures. Since unloading, melt, and sublimation are competitive ablation processes, they strongly influence whether snow is returned to the atmosphere or reaches the ground.

Key limitations remain in measuring canopy snow sublimation using eddy correlation systems (Conway et al., 2018; Harding & Pomeroy, 1996; Harvey et al., 2025; Helgason & Pomeroy, 2012b; Parviainen & Pomeroy, 2000) and separating snow unloading from meltwater drip (Floyd, 2012; Storck et al., 2002), which limit the development and testing of canopy snow ablation parameterisations. Whilst separating initial interception and ablation processes (Cebulski & Pomeroy, 2025a; Cebulski & Pomeroy, 2025b), will improve process representations, these routines still need to be evaluated together against additional field observations. Incorporating the updated unloading schemes developed here could improve the representation of canopy snow ablation and, by extension, the partitioning of precipitation and canopy albedo in hydrological and land surface models. Nonetheless, further testing is needed across different sites, climates, forest types, and spatial scales to assess model transferability and performance.

5 Conclusions

Canopy snow ablation processes govern the timing and partitioning of snowfall to the ground versus the atmosphere in forested environments, yet their representation in modelling frameworks remains uncertain due to insufficient process-level validation. This study evaluates existing canopy snow ablation theories using in-situ measurements of canopy snow load, unloading, and drip combined with a novel canopy snow energy and mass balance model. These observations revealed that canopy snow load, wind shear stress, and canopy snowmelt were statistically significant predictors

of snow unloading, collectively explaining 80% of its variability. In addition to this empirical evidence, physical processes such as structural degradation, snow particle bond weakening, lubrication of wet canopy snow during melt, and the shear force exerted on canopy snow by wind further support representing these processes. Although some studies use air temperature as an index of unloading resulting from canopy snowmelt and potential branch bending, here energy balance methodologies show improved performance in simulating canopy load during melt events.

Previous studies have demonstrated relationships between unloading and snow load, wind speed, and canopy snowmelt rate, but these processes have not been evaluated collectively. This study represents the first development and validation of an unloading model addressing both energy balance-based melt and dry snow unloading processes together. Novel parameterisations for dry snow and melt-induced unloading were introduced, with key differences from previously established approaches. Shear stress was found to be a stronger predictor of dry snow unloading ($R^2 = 0.61$) than wind speed ($R^2 = 0.54$) for non-melt periods. The canopy melt rate exerted the strongest control on snow unloading during melt events, consistent with one existing model. A new finding was that the ratio of unloading to canopy snowmelt increased with canopy snow load. Additionally, an existing approach which used the concept of a maximum intercepted snow load greatly underestimated the canopy snow storage capacity when compared to observed snow loads from weighed tree measurements. Throughout the two-years of observations presented here, a maximum canopy snow load was not observed, likely as unloading rates increased with higher snow loads. Wind transport events were relatively rare in this wind-exposed subalpine forest, but resulted in a considerable underestimation of the amount of snow returned to the atmosphere or surrounding sites during one event.

A new canopy snow ablation model that integrates an updated canopy snow mass and energy balance demonstrated improved accuracy across varied meteorological conditions compared to existing approaches. Existing models failed to maintain accuracy across events with a wide range of meteorology due to neglect of key processes and/or empirical representations of melt processes. The greatest inter-model discrepancies in canopy snow load occurred during warm and humid events, where temperature-based canopy snowmelt parameterisations showed substantially higher mean biases relative to energy balance-based models.

Amongst the models tested, the largest errors were found during cold & dry unloading events—though performance was improved when incorporating a site-specific shear stress-based parameterisation. Partitioning of intercepted snow disposition

between the ground and atmosphere varied most amongst cold events, where neglecting the dry snow unloading process resulted in considerable overestimates of canopy snow sublimation losses. All canopy snow models had greater consistency in partitioning canopy snow during warm & humid events, where all canopy snow was typically unloaded or melted as drip towards the ground surface. However, the rate of unloading was best represented by energy balance-based canopy snowmelt routines compared to empirical relationships. Although improved performance was found for the updated canopy snow ablation model compared to existing methods, across a wide range of meteorological conditions, additional testing across various climate and forest compositions is required to assess model transferability.

6 Acknowledgements

We acknowledge financial support from the University of Saskatchewan Dean's Scholarship, the Natural Sciences and Engineering Research Council of Canada's Discovery Grants, the Canada First Research Excellence Fund's Global Water Futures Programme, Environment and Climate Change Canada, Alberta Innovates Water Innovation Program, the Canada Foundation for Innovation's Global Water Futures Observatories facility, and the Canada Research Chairs Programme. We thank Madison Harasyn, Hannah Koslowsky, Kieran Lehan, Lindsey Langs and Fortress Mountain Resort for their help in the field and Tom Brown and Logan Fang for support of the CRHM platform.

7 Data & Software Availability Statement

The Cold Regions Hydrological Model Platform (CRHM) source code is available at https://github.com/srlabUsask/crhmcode. Model forcing data, model outputs, validation data, processed data, and scripts are available at https://doi.org/10.5281/zenodo.16898881.

References

Allan, R., Pereira, L., Raes, D., & Smith, M. (1998). *Crop evapotranspiration Guidelines for computing crop water requirements*. Food and Agriculture Organization of the United Nations.

Andreadis, K. M., Storck, P., & Lettenmaier, D. P. (2009). Modeling snow accumulation and ablation processes in forested environments. *Water Resources Research*, *45*(5), 1–33. https://doi.org/10.1029/2008WR007042

Aubry-Wake, C., & Pomeroy, J. W. (2023). Predicting hydrological change in an alpine glacierized basin and its sensitivity to landscape evolution and meteorological forcings. *Water Resources Research*, *59*(9). https://doi.org/10.1029/2022WR033363

Baggi, S., & Schweizer, J. (2008). Characteristics of wet-snow avalanche activity: 20 years of observations from a high alpine valley (Dischma, Switzerland). *Natural Hazards*, *50*(1), 97–108. https://doi.org/10.1007/s11069-008-9322-7

Bartlett, P. A., & Verseghy, D. L. (2015). Modified treatment of intercepted snow improves the simulated forest albedo in the Canadian Land Surface Scheme. *Hydrological Processes*, *29*(14), 3208–3226. https://doi.org/10.1002/HYP.10431

Berndt, H. W., & Fowler, W. B. (1969). Rime and hoarfrost in upper-slope forests of eastern washington. *Journal of Forestry*, *67*(2), 92–95. https://doi.org/10.1093/jof/67.2.92

Cebulski, A. C., & Pomeroy, J. W. (2025a). Theoretical Underpinnings of Snow Interception and Canopy Snow Ablation Parameterisations. *WIREs Water*, *12*, e70010. https://doi.org/10.1002/wat2.70010

Cebulski, A. C., & Pomeroy, J. W. (2025b). Snow Interception Relationships With Meteorology and Canopy Density. *Hydrological Processes*, *39*(4), e70135. https://doi.org/10.1002/hyp.70135

Clark, M. P., Nijssen, B., Lundquist, J. D., Kavetski, D., Rupp, D. E., Woods, R. A., Freer, J. E., Gutmann, E. D., Wood, A. W., Gochis, D. J., Rasmussen, R. M., Tarboton, D. G., Mahat, V., Flerchinger, G. N., & Marks, D. G. (2015). A unified approach for process-based hydrologic modeling: 2. Model implementation and case studies. *Water Resources Research*, *51*(4), 2515–2542. https://doi.org/10.1002/2015WR017200

Conway, J. P., Pomeroy, J. W., Helgason, W. D., & Kinar, N. J. (2018). Challenges in modeling turbulent heat fluxes to snowpacks in forest clearings. *Journal of Hydrometeorology*, *19*(10), 1599–1616. https://doi.org/10.1175/JHM-D-18-0050.1

Ellis, C. R., Pomeroy, J. W., Brown, T., & MacDonald, J. (2010). Simulation of snow accumulation and melt in needleleaf forest environments. *Hydrology and Earth System Sciences*, *14*(6), 925–940. https://doi.org/10.5194/hess-14-925-2010

Essery, R., Pomeroy, J. W., Parviainen, J., & Storck, P. (2003). Sublimation of snow from coniferous forests in a climate model. *Journal of Climate*, *16*(11), 1855–1864. https://doi.org/10.1175/1520-0442(2003)016%3C1855:SOSFCF%3E2.0.CO;2

Fang, X., & Pomeroy, J. W. (2023). Simulation of the impact of future changes in climate on the hydrology of Bow River headwater basins in the Canadian Rockies. *Journal of Hydrology*, *620*, 129566. https://doi.org/10.1016/j.jhydrol.2023.129566

Floyd, W. C. (2012). *Snowmelt energy flux recovery during rain-on-snow in regenerating forests* (p. 180) [PhD thesis, University of British Columbia]. https://doi.org/https://dx.doi.org/10.14288/1.0073024

Gelfan, A. N., Pomeroy, J. W., & Kuchment, L. S. (2004). Modeling forest cover influences on snow accumulation, sublimation, and melt. *Journal of Hydrometeorology*, *5*(5), 785–803. https://doi.org/10.1175/1525-7541(2004)005%3C0785:MFCIOS%3E2.0.CO;2

Harder, P., & Pomeroy, J. W. (2013). Estimating precipitation phase using a psychrometric energy balance method. *Hydrological Processes*, *27*(13), 1901–1914. https://doi.org/10.1002/hyp.9799

Harding, R. J., & Pomeroy, J. W. (1996). The Energy Balance of the Winter Boreal Landscape. *Journal of Climate*, *9*(11), 2778–2787. https://www.jstor.org/stable/26201420

Harvey, N., Burns, S. P., Musselman, K. N., Barnard, H., & Blanken, P. D. (2025). Identifying Canopy Snow in Subalpine Forests: A Comparative Study of Methods. *Water Resources Research*, *61*(1), e2023WR036996. https://doi.org/10.1029/2023WR036996

Hedstrom, N. R., & Pomeroy, J. W. (1998). Measurements and modelling of snow interception in the boreal forest. *Hydrological Processes*, *12*(10-11), 1611–1625. https://doi.org/10.1002/(SICI)1099-1085(199808/09)12:10/11%3C1611::AID-HYP684%3E3.0.CO;2-4

Helgason, W., & Pomeroy, J. W. (2012a). Characteristics of the near-surface boundary layer within a mountain valley during winter. *Journal of Applied Meteorology and Climatology*, *51*(3), 583–597. https://doi.org/10.1175/JAMC-D-11-058.1

Helgason, W., & Pomeroy, J. W. (2012b). Problems closing the energy balance over a homogeneous snow cover during midwinter. *Journal of Hydrometeorology*, *13*(2), 557–572. https://doi.org/10.1175/JHM-D-11-0135.1

Hoover, M. D., & Leaf, C. F. (1967). Processs and Significance of Interception in Colorado Subalpine Forest. *Proceeding of a National Science Foundation Advanced Science Seminar*.

Immerzeel, W. W., Lutz, A. F., Andrade, M., Bahl, A., Biemans, H., Bolch, T., Hyde, S., Brumby, S., Davies, B. J., Elmore, A. C., Emmer, A., Feng, M., Fernández, A., Haritashya, U., Kargel, J. S., Koppes, M., Kraaijenbrink, P. D. A., Kulkarni, A. V., Mayewski, P. A., … Baillie, J. E. M. (2020). Importance and vulnerability of the world's water towers. *Nature*, *577*(7790), 364–369. https://doi.org/10.1038/s41586-019-1822-y

Katsushima, T., Kato, A., Aiura, H., Nanko, K., Suzuki, S., Takeuchi, Y., & Murakami, S. (2023). Modelling of snow interception on a Japanese cedar canopy based on weighing tree experiment in a warm winter region. *Hydrological Processes*, *37*(6), 1–16. https://doi.org/10.1002/hyp.14922

Kesselring, J., Morsdorf, F., Kükenbrink, D., Gastellu-Etchegorry, J.-P., & Damm, A. (2024). Diversity of 3D APAR and LAI dynamics in broadleaf and coniferous forests: Implications for the interpretation of remote sensing-based products. *Remote Sensing of Environment*, *306*, 114116. https://doi.org/10.1016/j.rse.2024.114116

Kim, E., Gatebe, C., Hall, D., Newlin, J., Misakonis, A., Elder, K., Marshall, H. P., Hiemstra, C., Brucker, L., De Marco, E., Crawford, C., Kang, D. H., & Entin, J. (2017). NASA's snowex campaign: Observing seasonal snow in a forested environment. *2017 IEEE International Geoscience and Remote Sensing Symposium (IGARSS)*, 1388–1390. https://doi.org/10.1109/IGARSS.2017.8127222

Kozak, A., & Kozak, R. A. (1995). Notes on regression through the origin. *Forestry Chronicle*, *71*(3), 326–330. https://doi.org/10.5558/tfc71326-3

Krinner, G., Derksen, C., Essery, R., Flanner, M., Hagemann, S., Clark, M. P., Hall, A., Rott, H., Brutel-Vuilmet, C., Kim, H., Ménard, C. B., Mudryk, L., Thackeray, C., Wang, L., Arduini, G., Balsamo, G., Bartlett, P., Boike, J., Boone, A., … Zhu, D. (2018). ESM-SnowMIP: Assessing snow models and quantifying snow-related climate feedbacks. *Geoscientific Model Development*, *11*(12), 5027–5049. https://doi.org/10.5194/gmd-11-5027-2018

López-Moreno, J. I., Zabalza, J., Vicente-Serrano, S. M., Revuelto, J., Gilaberte, M., Azorin-Molina, C., Morán-Tejeda, E., García-Ruiz, J. M., & Tague, C. (2014). Impact of climate and land use change on water availability and reser-

voir management: Scenarios in the Upper Aragón River, Spanish Pyrenees. *Science of The Total Environment*, *493*, 1222–1231. https://doi.org/10.1016/j.scitotenv.2013.09.031

Lumbrazo, C., Bennett, A., Currier, W. R., Nijssen, B., & Lundquist, J. (2022). Evaluating multiple canopy-snow unloading parameterizations in SUMMA with time-lapse photography characterized by citizen scientists. *Water Resources Research*, *58*(6), 1–22. https://doi.org/10.1029/2021WR030852

Lundquist, J. D., Dickerson-Lange, S., Gutmann, E., Jonas, T., Lumbrazo, C., & Reynolds, D. (2021). Snow interception modelling: Isolated observations have led to many land surface models lacking appropriate temperature sensitivities. *Hydrological Processes*, *35*(7), 1–20. https://doi.org/10.1002/hyp.14274

MacDonald, J. P. (2010). *Unloading of intercepted snow in conifer forests* (p. 93) [M.{{Sc}}. Thesis]. Department of Geography, University of Saskatchewan.

Parviainen, J., & Pomeroy, J. W. (2000). Multiple-scale modelling of forest snow sublimation: Initial findings. *Hydrological Processes*, *14*(15), 2669–2681. https://doi.org/10.1002/1099-1085(20001030)14:15%3C2669::AID-HYP85%3E3.0.CO;2-Q

Pomeroy, J. W., Brown, T., Fang, X., Shook, K. R., Pradhananga, D., Armstrong, R., Harder, P., Marsh, C., Costa, D., Krogh, S. A., Aubry-Wake, C., Annand, H., Lawford, P., He, Z., Kompanizare, M., & Moreno, J. I. L. (2022). The cold regions hydrological modelling platform for hydrological diagnosis and prediction based on process understanding. *Journal of Hydrology*, *615*(128711), 1–25. https://doi.org/10.1016/j.jhydrol.2022.128711

Pomeroy, J. W., & Gray, D. M. (1995). *Snowcover Accumulation, Relocation and Management* (NHRI Science Report No. 7, p. 144). National Hydrology Research Institute, Environment Canada, Saskatoon, Canada.

Pomeroy, J. W., Gray, D. M., Hedstrom, N. R., & Janowicz, J. R. (2002). Prediction of seasonal snow accumulation in cold climate forests. *Hydrological Processes*, *16*(18), 3543–3558. https://doi.org/10.1002/hyp.1228

Pomeroy, J. W., Gray, D. M., Shook, K. R., Toth, B., Essery, R. L. H. H., Pietroniro, A., & Hedstrom, N. (1998a). An evaluation of snow accumulation and ablation processes for land surface modelling. *Hydrological Processes*, *12*(15), 2339–2367. https://doi.org/10.1002/(SICI)1099-1085(199812)12:15%3C2339::AID-HYP800%3E3.0.CO;2-L

Pomeroy, J. W., Marks, D., Link, T., Ellis, C. R., Hardy, J., Rowlands, A., & Granger, R. (2009). The impact of coniferous forest temperature on incom-

ing longwave radiation to melting snow. *Hydrological Processes*, *23*, 2513–2525. https://doi.org/10.1002/hyp.7325

Pomeroy, J. W., Parviainen, J., Hedstrom, N., & Gray, D. M. (1998b). Coupled modelling of forest snow interception and sublimation. *Hydrological Processes*, *12*(15), 2317–2337. https://doi.org/10.1002/(SICI)1099-1085(199812)12:15%3C2317::AID-HYP799%3E3.0.CO;2-X

Pomeroy, J. W., & Schmidt, R. A. (1993). The use of fractal geometry in modelling intercepted snow accumulation and sublimation. *Eastern Snow Conference*, *50*, 231–239.

Roesch, A., Wild, M., Gilgen, H., & Ohmura, A. (2001). A new snow cover fraction parameterization for the ECHAM4 GCM. *Climate Dynamics*, *17*(12), 933–946. https://doi.org/10.1007/s003820100153

Rutter, N., Essery, R., Pomeroy, J. W., Altimir, N., Andreadis, K. M., Baker, I., Barr, A., Bartlett, P., Boone, A., Deng, H., Douville, H., Dutra, E., Elder, K., Ellis, C. R., Feng, X., Gelfan, A., Goodbody, A., Gusev, Y., Gustafsson, D., … Yamazaki, T. (2009). Evaluation of forest snow processes models (SnowMIP2). *Journal of Geophysical Research: Atmospheres*, *114*(D6), 10–18. https://doi.org/10.1029/2008JD011063

Safa, H., Krogh, S. A., Greenberg, J., Kostadinov, T. S., & Harpold, A. A. (2021). Unraveling the controls on snow disappearance in montane conifer forests using multi-site lidar. *Water Resources Research*, *57*(12), 1–20. https://doi.org/10.1029/2020WR027522

Sanmiguel-Vallelado, A., López-Moreno, J. I., Morán-Tejeda, E., Alonso-González, E., Navarro-Serrano, F. M., Rico, I., & Camarero, J. J. (2020). Variable effects of forest canopies on snow processes in a valley of the central Spanish Pyrenees. *Hydrological Processes*, *34*(10), 2247–2262. https://doi.org/10.1002/hyp.13721

Sanmiguel-Vallelado, A., McPhee, J., Esmeralda Ojeda Carreño, P., Morán-Tejeda, E., Julio Camarero, J., & López-Moreno, J. I. (2022). Sensitivity of forest–snow interactions to climate forcing: Local variability in a Pyrenean valley. *Journal of Hydrology*, *605*. https://doi.org/10.1016/j.jhydrol.2021.127311

Schmidt, R. A., & Gluns, D. R. (1991). Snowfall interception on branches of three conifer species. *Canadian Journal of Forest Research*, *21*(8), 1262–1269. https://doi.org/10.1139/x91-176

Schmidt, R. A., & Pomeroy, J. W. (1990). Bending of a conifer branch at subfreezing temperatures: Implications for snow interception. *Canadian Journal of Forest Research*, *20*(8), 1251–1253. https://doi.org/10.1139/x90-165

Sicart, J. E., Pomeroy, J. W., Essery, R. L. H., & Bewley, D. (2006). Incoming longwave radiation to melting snow: Observations, sensitivity and estimation in Northern environments. *Hydrological Processes*, *20*(17), 3697–3708.

Staines, J., & Pomeroy, J. W. (2023). Influence of forest canopy structure and wind flow on patterns of sub-canopy snow accumulation in montane needleleaf forests. *Hydrological Processes*, *37*(10), 1–19. https://doi.org/10.1002/hyp.15005

Storck, P., Lettenmaier, D. P., & Bolton, S. M. (2002). Measurement of snow interception and canopy effects on snow accumulation and melt in a mountainous maritime climate, Oregon, United States. *Water Resources Research*, *38*(11), 1–16. https://doi.org/10.1029/2002wr001281

Szczypta, C., Gascoin, S., Houet, T., Hagolle, O., Dejoux, J.-F., Vigneau, C., & Fanise, P. (2015). Impact of climate and land cover changes on snow cover in a small Pyrenean catchment. *Journal of Hydrology*, *521*, 84–99. https://doi.org/10.1016/j.jhydrol.2014.11.060

Troendle, C. A. (1983). The potential for water yield augmentation from forest management in the Rocky Mountain region. *Journal of the American Water Resources Association*, *19*(3), 359–373. https://doi.org/10.1111/j.1752-1688.1983.tb04593.x

Valante, F., David, J. S., & Gash, J. H. C. (1997). Modelling interception loss for two sparse eucalypt and pine forests in central Portugal using reformulated Rutter and Gash analytical models. *Journal of Hydrology*, *190*(1-2), 141–162. https://doi.org/10.1016/S0022-1694(96)03066-1

Verseghy, D. L. (2017). *Class – the Canadian Land Surface Scheme (version 3.6.1) technical documentation.* (January; p. 174). Environment and Climate Change Canada Internal Rep.

Viviroli, D., Kummu, M., Meybeck, M., Kallio, M., & Wada, Y. (2020). Increasing dependence of lowland populations on mountain water resources. *Nature Sustainability*, *3*(11), 917–928. https://doi.org/10.1038/s41893-020-0559-9

Weiskittel, A. R., Kershaw, J. A., Hofmeyer, P. V., & Seymour, R. S. (2009). Species differences in total and vertical distribution of branch- and tree-level leaf area for the five primary conifer species in Maine, USA. *Forest Ecology and Management*, *258*(7), 1695–1703. https://doi.org/10.1016/j.foreco.2009.07.035

Wheater, H. S., Pomeroy, J. W., Pietroniro, A., Davison, B., Elshamy, M., Yassin, F., Rokaya, P., Fayad, A., Tesemma, Z., Princz, D., Loukili, Y., DeBeer, C. M., Ireson, A. M., Razavi, S., Lindenschmidt, K.-E., Elshorbagy, A., MacDonald, M., Abdelhamed, M., Haghnegahdar, A., & Bahrami, A. (2022). Ad-

vances in modelling large river basins in cold regions with Modélisation Environmentale Communautaire—Surface and Hydrology (MESH), the Canadian hydrological land surface scheme. *Hydrological Processes*, *36*(4), 1–24. https://doi.org/10.1002/hyp.14557

Zhong, F., Jiang, S., van Dijk, A. I. J. M., Ren, L., Schellekens, J., & Miralles, D. G. (2022). Revisiting large-scale interception patterns constrained by a synthesis of global experimental data. *Hydrology and Earth System Sciences*, *26*(21), 5647–5667. https://doi.org/10.5194/hess-26-5647-2022